A&A 499, 917–921 (2009)
DOI: 10.1051/0004-6361/200810710

Astronomy & Astrophysics

Dynamic Lyα jets

J. Koza[1], R. J. Rutten[2,3], and A. Vourlidas[4]

[1] Astronomical Institute, Slovak Academy of Sciences, 059 60 Tatranská Lomnica, Slovakia
e-mail: koza@astro.sk
[2] Sterrekundig Instituut, Universiteit Utrecht, PO Box 80 000, 3508 TA Utrecht, The Netherlands
[3] Institute of Theoretical Astrophysics, University of Oslo, PO Box 1029, Blindern, 0315 Oslo, Norway
[4] Code 7663, Naval Research Laboratory, Washington, DC 20375, USA

Received 30 July 2008 / Accepted 13 February 2009

ABSTRACT

Context. The solar chromosphere and transition region are highly structured and complex regimes. A recent breakthrough has been the identification of dynamic fibrils observed in Hα as caused by field-aligned magnetoacoustic shocks.
Aims. We seek to find whether such dynamic fibrils are also observed in Lyα.
Methods. We used a brief sequence of four high-resolution Lyα images of the solar limb taken by the Very high Angular resolution ULtraviolet Telescope (VAULT), which displays many extending and retracting Lyα jets. We measured their top trajectories and fitted parabolas to the 30 best-defined ones.
Results. Most jet tops move supersonically. Half of them decelerate, sometimes superballistically, the others accelerate. This bifurcation may arise from incomplete sampling of recurrent jets.
Conclusions. The similarities between dynamic Lyα jets and Hα fibrils suggest that the magnetoacoustic shocks causing dynamic Hα fibrils also affect dynamic Lyα jets.

Key words. Sun: transition region – Sun: UV radiation

1. Introduction

The solar chromosphere observed in Hα is a bewildering mass of elongated features, but a breakthrough concerning so-called dynamic fibrils (henceforth Hα DFs) has been made in the studies of De Pontieu et al. (2004, 2007a), Hansteen et al. (2006), Rouppe van der Voort et al. (2007), Heggland et al. (2007), and Langangen et al. (2008a,c) following earlier work by Suematsu et al. (1995). These studies have established that Hα DFs, which are rows of dark fibrilar features jutting out from plage and network with periodic extension and retraction, display repetitive mass loading by upward propagating magnetoacoustic shock waves driven by the global solar oscillations. Reduction of the effective gravity along tilted magnetic channels lowers their cut-off frequency and lets them propagate into the chromosphere, steepen into shocks, and repetitively lift the chromospheric-transition region interface.

These studies are all based on optical observations, but de Wijn & De Pontieu (2006) have studied transition-region jets in C IV in ultraviolet TRACE images and found remarkable morphological similarities between Hα DFs and their C IV counterparts. The DFs may represent the injection of cool material postulated by Judge (2008) as the source of hot sheaths making up the transition region.

In this paper we report the presence of similar features in solar Lyα images taken with the Very high Angular resolution ULtraviolet Telescope (VAULT, Korendyke et al. 2001) during its second rocket flight. VAULT acquired Lyα images with much higher spatial and temporal resolution than the EUV imagery from the TRACE, SoHO, and STEREO satellites but only for a few minutes. The Lyα fine structure in these images is discussed by Patsourakos et al. (2007) and Judge & Centeno (2008). Here we locate and study extending or retracting Lyα brightness structures in images taken near the limb. We call these dynamic Lyα jets, abbreviated to Lyα DJs, and compare them to Hα DFs.

2. Observations and measurements

We used Lyα images[1] recorded during the second VAULT flight of 14 June 2002. The cadence was 17 s, the exposure time 1 s, the image scale 0.124 arcsec px^{-1}, and the angular resolution 1/3 arcsec. The VAULT gratings isolated a 150 Å wide spectral band around Lyα and a narrow-band filter reduced the passband to 72 Å *FWHM*. The resulting signal is about 95% pure Lyα emission (Teriaca & Schühle, personal communication). More detail is given in Korendyke et al. (2001) and Patsourakos et al. (2007).

The VAULT-II flight recorded two Lyα image sequences, a seventeen-image one stepping over an extended active area on the disk and a four-image one of quieter areas near the limb. We use only the four limb images because Lyα jets are best observed as bright features in projection against the dark internetwork background. The four images were precisely co-aligned through cross-correlation using routines of P. Sütterlin. We then applied appropriate greyscaling to enhance their fine structure and used extensive visual inspection to identify Lyα jets and to study their temporal behavior. They are similar to limb spicules in being bright against dark internetwork and in showing hedgerow-clustering at network boundaries. Similar Lyα jets are also seen in the disk sequence, but we decided to limit our measurements

[1] The VAULT data archives are available at http://wwwsolar.nrl.navy.mil/rockets/vault/.

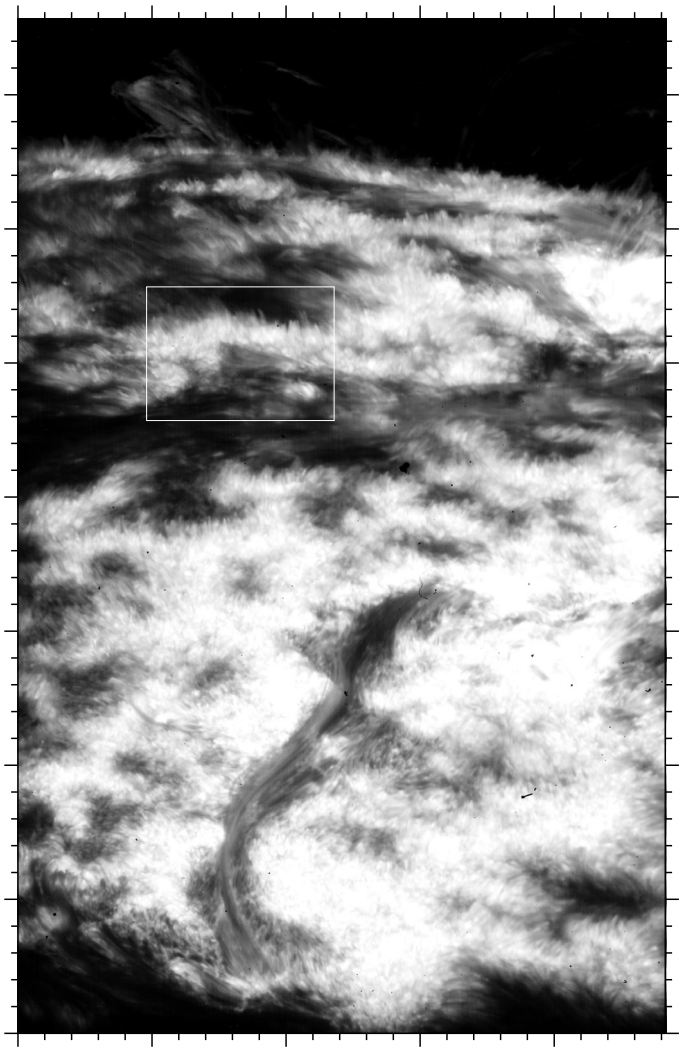

Fig. 1. Lyα image taken at 18:16:56 UT covering the east limb. We invite the reader to inspect this image at large magnification with a pdf viewer. Lyα jets are grouped in hedgerows at network boundaries that are best seen in projection against the dark internetwork. The rectangle selects the hedgerow enlarged in Fig. 2. The contrast is enhanced by logarithmic brightness scaling. Tickmark spacing: 10 arcsec.

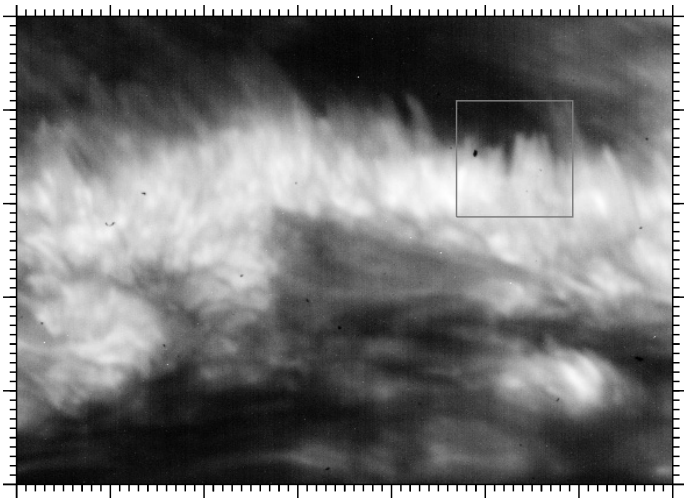

Fig. 2. Enlargement of the subfield outlined in Fig. 1. The rectangle outlines the smaller subfield shown in Fig. 4 with Lyα DJs 3 and 11. Tickmark spacing: 1 arcsec.

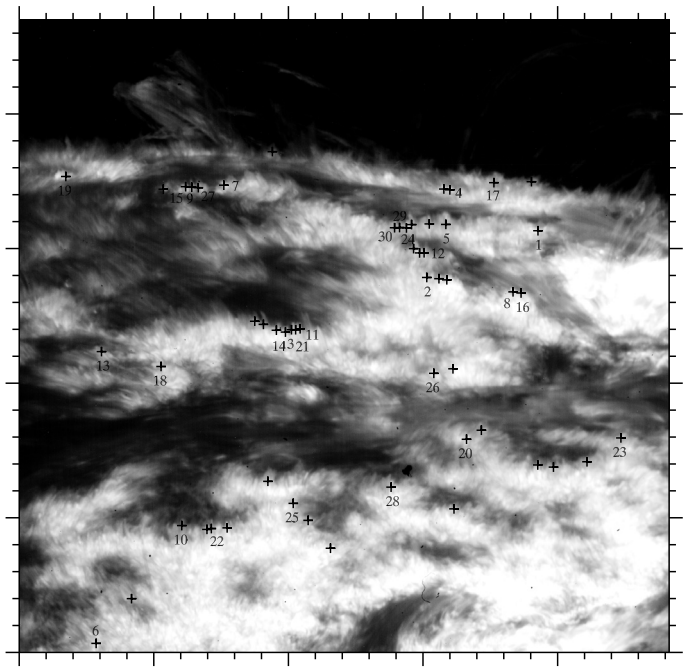

Fig. 3. The upper part of Fig. 1 with 55 Lyα DJs marked by plus signs. The 30 DJs selected for further analysis are labeled with their reference number. Tickmark spacing: 10 arcsec.

to the limb sequence that shows them best. It clearly shows temporal variation in the spatial extent of many Lyα jets, even during the brief one-minute sequence duration.

The four images used here were taken between 18:16:56 and 18:17:47 UT at the east limb. The first is shown in Fig. 1. Towards the limb it displays thick hedgerows of bright Lyα jets, jutting out at network boundaries. They are remarkably similar, at reversed contrast, to the dark hedgerows in filtergrams taken in the wings of Hα (e.g., Fig. 9.1 of Stix 2004 and Fig. 7 of Rutten 2007), in which Dopplershift of the line core into the wings selects dynamic fibrils over the quiescent network-spanning fibrils that dominate the scene at Hα line center. Such extended fibrils appear dark in the VAULT-II images and provide the background against which the hedgerows appear bright. Figure 2 shows an enlargement of one such hedgerow. The individual jets have widths of only one arcsec or less, requiring VAULT's high resolution for identification and tracking.

We have manually identified 55 Lyα jets that exhibit measurable extension and/or retraction during the four-frame sequence, all located in network clusters with convenient dark backgrounds. More weeding, described below, resulted in the selection of 30 of these Lyα DJs for presentation. They are marked by their reference number in Fig. 3. Some examples are shown in Fig. 4 in the form of small cutout sequences from the four frames. There are many other features with similar morphology in Fig. 3; undoubtedly, many more might be recognized as Lyα DJs in longer time sequences. However, there are also many jet-like features that do not change at all during the brief sequence duration. For example, the conspicuous jet to the right of retracting Lyα DJ 24 in the bottom panels of Fig. 4 does not show any change.

The cutouts in Fig. 4 illustrate that these Lyα DJs appear rather fuzzy, making measurement of their extension or retraction somewhat imprecise. At the suggestion of the referee to an earlier version of this paper, we developed a measuring method that includes error estimation. We first defined reference

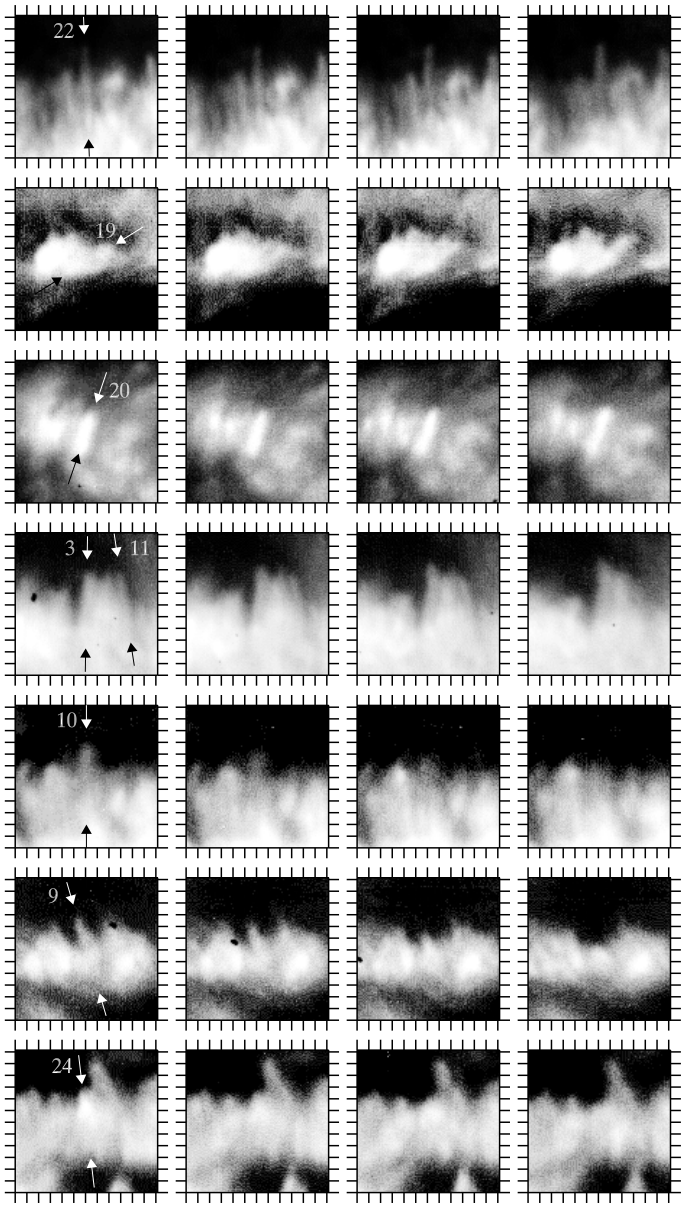

Fig. 4. Time evolution of extending (Nos. 22, 19, 20, 3) and retracting (Nos. 11, 10, 9, 24) Lyα DJs. The time increases with 17-s intervals between the columns. The arrows define the jet axis. The tickmarks have 1-arcsec spacing.

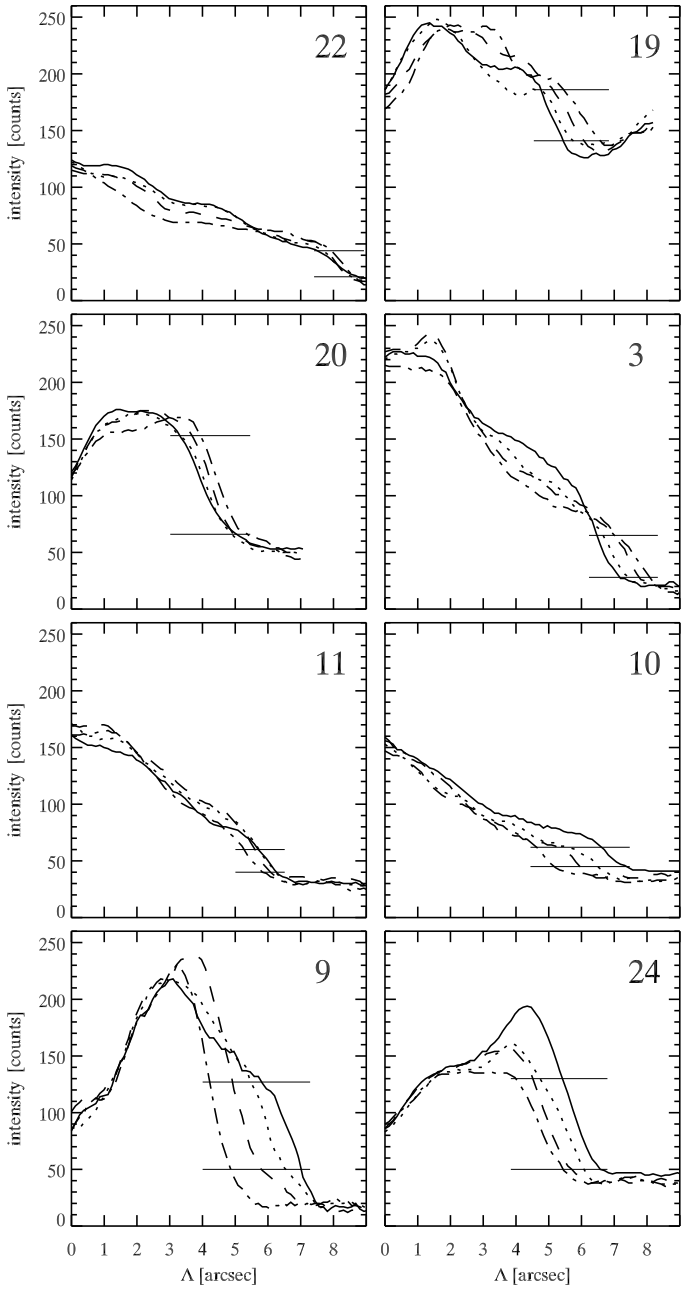

Fig. 5. Intensity profiles along the longitudinal axes of the Lyα DJs shown in Fig. 4. The solid, dotted, dashed, and dashed-dotted curves correspond to the 1st, 2nd, 3rd, and 4th panel in the corresponding row of Fig. 4, respectively, and show the temporal evolution. The thin-line markers specify the ranges of intensity thresholds defining each jet top. The reference footpoints with $\Lambda = 0$ are fixed in time.

footpoints and longitudinal axis orientations for each of the 55 Lyα DJs to measure their lengths. Since many jets have no clear base due to crowding in the network from which they originate, the footpoint designation is rather arbitrary but this does not affect our length change measurements since we maintained the same footpoint for the three other frames after selecting it in the first frame. We similarly maintained the axis direction. No correction for projection effects was applied. The limbward viewing suggests that, on average, these Lyα DJs are viewed more or less from aside.

We then plotted the intensities along each jet against a length coordinate Λ measured in arcsec along the axis from the footpoint at $\Lambda = 0$. Figure 5 shows the intensity profiles for the same Lyα DJs as displayed in Fig. 4. Each profile is box-car smoothed over 6 pixels (0.74 arcsec) to reduce noise. The differences between the four curves in each panel show the temporal jet evolution. The DJs in the upper four panels extend; i.e., their outer parts become brighter. Their lower parts sometimes weaken simultaneously (as for DJ 22 in the first panel). The DJs in the lower four panels retract, without much change in their lower parts. Inspection of all 55 plots made us discard 15 DJs for not showing such regular progression in their outer parts.

The question then was how to define the jet top locations in order to measure jet length variations in terms of their top displacements $\Delta\Lambda_{\rm top}(t)$. For each DJ we selected intensity thresholds at the onset of steep intensity decay with Λ and at the outer limit of visibility, as illustrated by horizontal dashes in Fig. 5. Picking an intensity value from such a range as the top location in one profile yields samples of $\Delta\Lambda_{\rm top}(t)$ for the other three

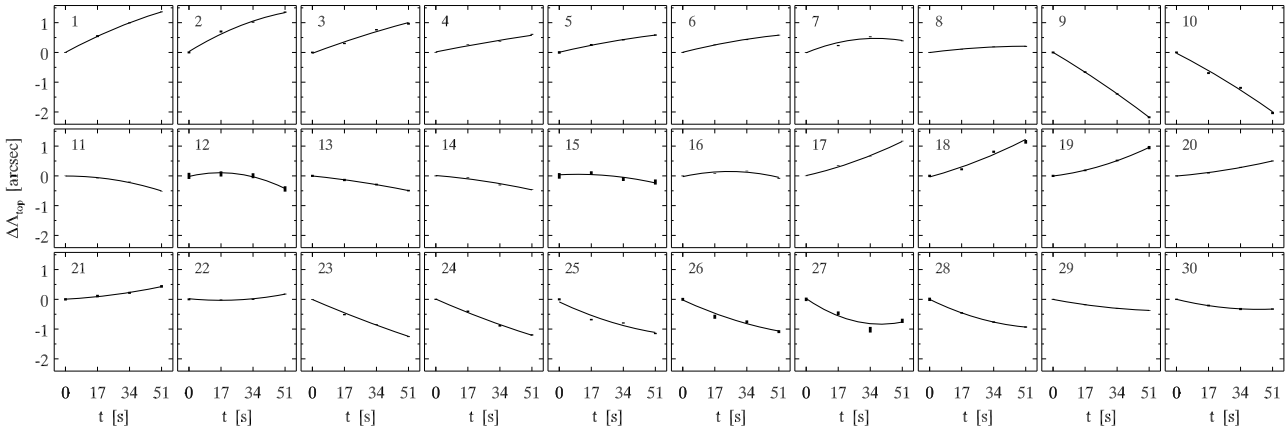

Fig. 6. Trajectory measurements $\Delta\Lambda_{\rm top}(t)$ of 30 jet tops along their axes. The heights of the symbols specify the error estimates. The solid curves are the parabolic fits. Nos. 1–16: decelerating jets showing extension (1–8) and retraction (9–16). Nos. 17–30: accelerating jets showing extension (17–22) and retraction (23–30).

Table 1. Lyα DJ excursion amplitudes and kinematic quantities.

Feature type		A [arcsec]	$\lvert a\rvert$ [m s^{-2}]	$v_{\rm max}$ [km s^{-1}]	T [min]
Lyα DJs	decelerating	0.6 (0.8±0.5) ⟨0.2, 2.2⟩	165 (235±173) ⟨44, 650⟩	13 (17±9) ⟨6, 35⟩	2.8 (3.3±2.2) ⟨0.9, 7.5⟩
	accelerating		246 (257±175) ⟨87, 797⟩	21 (18±7) ⟨9, 32⟩	not defined
Hα DFs		–	136 (146±56) ⟨40, 320⟩	18 (18±6) ⟨8, 35⟩	4.2 (4.8±1.4) ⟨2, 10.8⟩

The first number of each entry is the median value, followed by the mean with standard deviation (between parentheses) and the range (between angle brackets). The bottom row shows comparable determinations for Hα DFs from De Pontieu et al. (2007a).

by finding the displacement in Λ for the outermost pixel with that intensity. We automated this in a procedure using a random generator to pick threshold values from a normal distribution centered on and covering the selected range, and so obtained distributions of $\Delta\Lambda_{\rm top}(t)$ displacements for each jet that yield rms error estimates. This was repeated using each of the four frames as initial reference; the four error estimates were averaged. These errors represent the threshold-definition uncertainty and the amount of gradient divergence between the four profiles per jet. They are smallest when the curves are parallel, as in the case of DJ 9 in the bottom-left panel of Fig. 5.

Following the example of Hansteen et al. (2006) and De Pontieu et al. (2007a) we fitted the measured displacements, using the error estimates as weights, with parabolas $\Delta\Lambda_{\rm top}(t) = v_1\,(t-t_1) + (a/2)\,(t-t_1)^2$ where v_1 is the onset velocity (positive when upward) at the time t_1 at which the first frame was taken and a the deceleration (when negative) or acceleration (when positive). The terminal velocity v_4 at the time of the fourth frame is $v_4 = v_1 + a\,(t_4 - t_1)$ where $t_4 - t_1 = 51$ s.

Since the onset and terminal velocities v_1 and v_4 differ in all cases and can be negative, we define a maximum velocity $v_{\rm max}$ as the higher of $|v_1|$ and $|v_4|$. The apex of parabolic decelerated motion starting with $v_{\rm max}$ is reached after $v_{\rm max}/|a|$ seconds. We estimate the total jet excursion duration T for decelerating jets by doubling this value: $T = 2v_{\rm max}/|a|$. Since the four frames are likely to sample only part of a jet top trajectory, both $v_{\rm max}$ and T represent only lower limits.

Finally, we discarded 10 more DJs from our sample because the error estimates for their a and/or $v_{\rm max}$ determinations exceeded 100%.

3. Results

Figure 6 shows the top trajectory measurements, the corresponding error estimates, and the parabolic fits for the remaining 30 Lyα DJs. Table 1 specifies the average values of the trajectory amplitudes and the fit parameters together with their variances and ranges.

Most jet tops do not travel far during the short sequence duration, only over a median distance of 0.6 arcsec, but these travel measurements are nevertheless significant thanks to VAULT's 0.3-arcsec resolution. Some of the decelerating jets have significantly greater deceleration $-a$ than the solar surface gravity (274 m s^{-2}); we call these superballistic. The maximum velocity estimates $v_{\rm max}$ all but one exceed the chromospheric sound speed (8 km s^{-1}, e.g., Uitenbroek 2006). The excursion duration estimates T range from 1 to 7.5 min with a median at 2.8 min. Again, we emphasize that the last two parameters are likely to be underestimated when the brief image sequence did not cover the full jet-top excursion.

Figure 7 plots the maximum velocity amplitude $v_{\rm max}$ against the deceleration/acceleration amplitude $|a|$ for the selected 30 Lyα DJs. The scatter and the errors are large and the statistics low, but the plot suggests positive correlation between $v_{\rm max}$ and $|a|$ for both the decelerating and the accelerating Lyα DJs.

4. Discussion

Obviously, longer Lyα image sequences at the VAULT-II resolution are needed to gain better information than these four images provide. Nevertheless, they do show the existence of dynamic jets that fan out from network and extend or retract during the one-minute image sequence.

How do these Lyα DJs compare to the now well-studied and fairly well-explained Hα DFs? They have similar shapes, occupy similar locations on the solar surface, show similar hedge-row morphology, and extend or retract along their length the same way. The measurements for the 16 decelerating ones in Table 1 show fairly good correspondence with the Hα DF measurements listed at the bottom of the table. Figure 7 suggests a positive

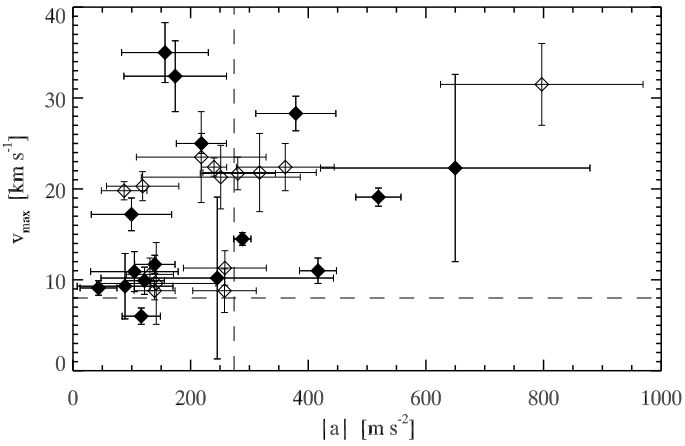

Fig. 7. Maximum velocity amplitude v_{max} against deceleration/acceleration amplitude $|a|$ for the selected 30 Lyα DJs. *Filled symbols*: decelerating DJs. *Empty symbols*: accelerating DJs. *Dashed lines*: chromospheric sound speed of 8 km s^{-1} and solar surface gravity.

correlation between v_{max} and $|a|$ comparable to the linear relations for Hα DFs. Our estimate of the mean Lyα DJ excursion duration is about one and half minutes shorter than the average Hα DF periodicity reported by De Pontieu et al. (2007a), but represents only a lower limit. Three of the sixteen DJs show substantially greater superballistic deceleration than the maximum of 320 m s^{-2} for DFs reported by De Pontieu et al. (2007a) and the maximum of 400 m s^{-2} reported by Rouppe van der Voort et al. (2007) and De Pontieu et al. (2007b) for quiet-Sun mottles and for type-1 spicules, respectively, but with large uncertainty for one of them. We conclude that, overall, our decelerating Lyα DJs are rather similar to Hα DFs.

However, in contrast to the Hα DF studies, we found a roughly equal number of Lyα DJs that significantly accelerate rather than decelerate. These are collected in the lower half of Fig. 6. The two sets of trajectories together suggest that they might actually be incomplete samples of sinusoidal motion or, as the referee has pointed out, sample the end of one shock-driven feature and the onset of the next one if these Lyα DJs occur in succession as Hα DFs do. Note that our length estimates do not differ significantly between the two sets, but these are rather arbitrary.

An obvious difference between Lyα DJs and Hα DFs is that the former appear bright against dark backgrounds, the latter dark against bright backgrounds. Lyα emissivity indicates the presence of gas that is sufficiently hot for collisional excitation of its upper level at 10.2 eV. Sufficient population of that level is also required to make fibrils opaque in Hα. The recent study by Leenaarts et al. (2007) suggests that cool fibrils may maintain much greater Hα opacity than their temperature would suggest if they have recently undergone shock heating. Hence, Hα DFs may remain opaque also when they are cool during part of their lifetime. They will be much more opaque in Lyα. Can the same fibril appear bright in Lyα and dark in Hα? Perhaps through hot-sheath topology of the transition region, with the latter surrounding cool DFs as hot shells (e.g., Rutten 2007; De Pontieu et al. 2007a). The neutral-hydrogen diffusion mechanism recently proposed by Judge (2008) seems a viable candidate. Detailed time-dependent numerical MHD simulation may demonstrate this. However, realistic evaluation of Hα formation from such simulations remains a formidable challenge that may be helped by constraints derived from Lyα.

Finally, the Lyα DJs studied here are likely related to chromospheric phenomena such as regular spicules (e.g. Sterling 2000), straws (Rutten 2006, 2007), and type-2 spicules (De Pontieu et al. 2007b; Langangen et al. 2008b).

Acknowledgements. We are indebted to P. Sütterlin for providing his image-alignment routines and to the referee whose comments improved the paper substantially. J. Koza thanks J. Rybák, P. Gömöry, and A. Kučera for valuable discussions and comments. His research was supported by EC Marie Curie European Re-Integration Grant MERG-CT-2007-046475 and by the Slovak Research and Development Agency APVV under contract APVV-0066-06. The VAULT development was supported by the Office of Naval Research (task area SP033-02-43) and NASA (defense procurement request S-84002F).

References

De Pontieu, B., Erdélyi, R., & James, S. P. 2004, Nature, 430, 536
De Pontieu, B., Hansteen, V. H., Rouppe van der Voort, L., van Noort, M., & Carlsson, M. 2007a, ApJ, 655, 624
De Pontieu, B., McIntosh, S. W., Hansteen, V. H., et al. 2007b, PASJ, 59, S655
de Wijn, A. G., & De Pontieu, B. 2006, A&A, 460, 309
Hansteen, V. H., De Pontieu, B., Rouppe van der Voort, L., van Noort, M., & Carlsson, M. 2006, ApJ, 647, L73
Heggland, L., De Pontieu, B., & Hansteen, V. H. 2007, ApJ, 666, 1277
Judge, P. 2008, ApJ, 683, L87
Judge, P. G., & Centeno, R. 2008, ApJ, 687, 1388
Korendyke, C. M., Vourlidas, A., Cook, J. W., et al. 2001, Sol. Phys., 200, 63
Langangen, Ø., Carlsson, M., Rouppe van der Voort, L., Hansteen, V., & De Pontieu, B. 2008a, ApJ, 673, 1194
Langangen, Ø., De Pontieu, B., Carlsson, M., et al. 2008b, ApJ, 679, L167
Langangen, Ø., Rouppe van der Voort, L., & Lin, Y. 2008c, ApJ, 673, 1201
Leenaarts, J., Carlsson, M., Hansteen, V., & Rutten, R. J. 2007, A&A, 473, 625
Patsourakos, S., Gouttebroze, P., & Vourlidas, A. 2007, ApJ, 664, 1214
Rouppe van der Voort, L. H. M., De Pontieu, B., Hansteen, V. H., Carlsson, M., & van Noort, M. 2007, ApJ, 660, L169
Rutten, R. J. 2006, in Solar MHD Theory and Observations: A High Spatial Resolution Perspective, ed. J. Leibacher, R. F. Stein, & H. Uitenbroek, ASP Conf. Ser., 354, 276
Rutten, R. J. 2007, in The Physics of Chromospheric Plasmas, ed. P. Heinzel, I. Dorotovič, & R. J. Rutten, ASP Conf. Ser., 368, 27
Sterling, A. C. 2000, Sol. Phys., 196, 79
Stix, M. 2004, The sun: an introduction, 2nd edn., Astronomy and astrophysics library (Berlin: Springer), ISBN: 3-540-20741-4
Suematsu, Y., Wang, H., & Zirin, H. 1995, ApJ, 450, 411
Uitenbroek, H. 2006, in Solar MHD Theory and Observations: A High Spatial Resolution Perspective, ed. J. Leibacher, R. F. Stein, & H. Uitenbroek, ASP Conf. Ser., 354, 313